Multistable Series Elastic Actuators: Design and Control

Leonardo Cappello[a,1,*], Michele Xiloyannis[b,1], Binh Khanh Dinh[c], Alberto Pirrera[d], Filippo Mattioni[e], Lorenzo Masia[f]

[a]*The BioRobotics Institute, Scuola Superiore Sant'Anna, Pisa, Italy.*
[b]*Sensory-Motor-Systems (SMS) Lab, ETH Zurich, Zurich, Switzerland.*
[c]*Biorobotics Lab, Department of Mechatronics, Ho Chi Minh University of Technology and Education, Ho Chi Minh, Vietnam.*
[d]*Bristol Composites Institute (ACCIS), Department of Aerospace Engineering, University of Bristol, Bristol, United Kingdom.*
[e]*Gurit Composites Engineering, Newport, United Kingdom.*
[f]*Institut für Technische Informatik (ZITI), Heidelberg University, Heidelberg, Germany.*

Abstract

In this paper we propose a novel actuation concept, consisting of a conventional DC motor in series with a compliant element having multiple configurations of equilibrium. The proposed device works similarly to a traditional series elastic actuator, where the elasticity increases safety and force control accuracy, but presents the possibility of achieving higher efficiency and releasing energy at a higher bandwidth. An introduction on the mechanical properties of the multistable element explains its working principle and provides simple model-based guidelines to its design. We characterize the actuator and propose a robust algorithm to control both storage and rate of release of its elastic energy. Using only an incremental encoder on the motor's axis, we show that we can reliably control the position of the actuator and its convergence towards a state of stable equilibrium. The proposed robust control architecture sensibly improves the tracking accuracy with respect to conventional PID controllers. Once reconfigured, no additional energy from the motor is required to hold the position, making the actuator appealing for energy-efficient systems. We conclude with a discussion on the limitations and advantages of such technology, suggesting avenues for its application in the field of assistive robotics.

Keywords: Series Elastic Actuators; Multistability; System Identification; Robust Position Control; Linear Kalman Filter.

1. Introduction

The robotic precept "the stiffer, the better", based on the assumption that rigid links in structural components assure higher performance, has long permeated the industrial automation community. In traditional position-controlled robotic systems, especially designed for fast assembly lines, the interface between the end-effector and the environment is designed to be rigid: a stiff transmission reduces undesired dynamic behaviors that may arise from deformable components and increases position-control bandwidth. However, as robots start to populate our warehouses, offices, hospitals and homes, their design requirements shift significantly. Robots that interact with human beings need to be gentle, compliant and safe, as well as fast and powerful [1].

A substantial number of works, starting from the early 80s, proposed to achieve safety in physical Human-Robot Interaction (pHRI) by means of active force controllers. Hogan's impedance controller [2] and Salisbury's stiffness control [3] are probably the most well-known attempts of getting a heavy, rigid, electromechanical system to behave gently as it interacts with the environment. Despite leading to pioneering results, these early studies also highlighted the limitations of "virtual" compliance: the impedance characteristics are limited in bandwidth by the performance of the controller and, since the hardware is intrinsically rigid, they are not robust to failure [4].

Later, Pratt *et al.* proposed to intentionally introduce mechanical compliance in the design [5]. Placing an elastic element between the actuator and the load effectively decouples the actuator's rotor inertia from the links, whenever an impact occurs. The authors indeed showed that, using this paradigm, one can increase shock tolerance and reduce inadvertent damage to the environment. Furthermore, Series Elastic Actuators (SEA) feature improved stability and accuracy in force control compared to rigid transmissions. This improvement is achieved by transforming a force control problem into a position control problem: force can be accurately inferred by sensing the deformation of the compliant element. Finally, one can exploit the energy-storage properties of compliant elements to increasing the efficiency and performance of the

*Corresponding author.
Email addresses: leonardo.cappello@santannapisa.it (Leonardo Cappello), m.xiloyannis@gmail.com (Michele Xiloyannis), khanhdb@hcmute.edu.vn (Binh Khanh Dinh), alberto.pirrera@bristol.ac.uk (Alberto Pirrera), filippo.mattioni@gmail.com (Filippo Mattioni), lormasia@gmail.com (Lorenzo Masia)
[1]These authors contributed equally to the paper.

actuator, especially in highly dynamic applications such as locomotion [6, 7].

The advantages of SEAs in pHRI pioneered a new frontier of flexible robotics. However, the compliance of typical elastic components is constant, hence, during operation, the apparent stiffness of the system cannot be adjusted. As it often happens in engineering, one can be inspired by the characteristics of nature that have survived the pitiless selection of evolution: humans continuously vary the compliance of their limbs between and within tasks [8].

The idea of adaptive stiffness spawned the design of Variable Stiffness Actuators (VSAs) [9], devices able to continuously tune the stiffness of the transmission during operation, allowing an accurate control of the dynamic characteristics of the interaction with the environment.

SEAs and VSAs guarantee a safer regulation of the interaction force [10, 11] and greatly simplify the control problem [12]. A common feature to SEAs and VSAs is the use of elastic elements having a single resting configuration. This results in the passive element having a monotonic elastic energy profile, shown in Figure 1.a.

An increasing number of studies are exploring the advantages of multistable flexible structures [13]. Unlike traditional elastic elements, these components have multiple stable configurations, offering appealing advantages, especially in highly dynamic tasks [14].

An elegant example of the convenience of architectures with multiple stability configurations can be found in nature. The *Dionaea muscipula*, commonly known as the venus flytrap, achieves the fastest known movement in the plant kingdom by exploiting the bistable structure of its leafs [15]. Forterre *at al.* have shown that this phenomenon is initiated by an active biochemical component that triggers an elastic transition of the leaf from a stable convex to a stable concave shape [15]; this happens in less than 100 ms, leaving no chance of escaping even to the fastest of insects. Once in its stable concave shape, no additional energy is needed to hold the leafs in position.

This mechanism effectively behaves like an actuator-multistable spring pair, where the actuator provides the energy to traverse the crest of an elastic potential hill of the spring, and the compliant structure snaps to the closest equilibrium. An electromechanical equivalent of this concept is shown in Figure 1.b. Once in a stable configuration, the system effectively behaves like a SEA.

The dynamic properties of a bistable structure were exploited by Santer *et al.* [16], to design an energy-efficient jumping device, using three nitinol spring actuators to trigger the forward and reverse transitions between stable states, and are extensively studied for aerospace applications, to design morphing structures for rotor blade flaps [17]. Plooij and Wisse have further shown a promising 20% reduction in the energetic cost of moving a robotic arm in repetitive tasks, by placing a nonlinear spring in parallel with electric motors [18].

In [19], Lachenal and colleagues proposed a bistable structure consisting of two pre-stressed carbon flanges,

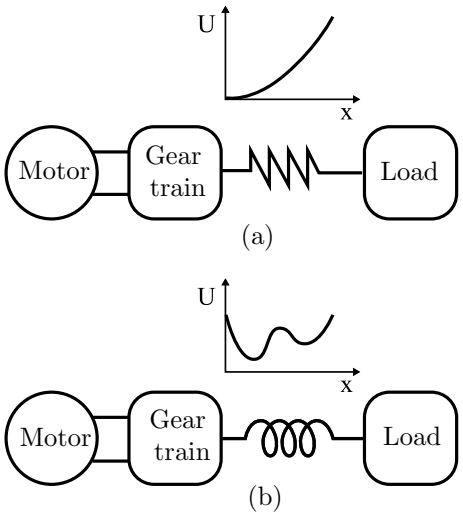

Figure 1: Series elastic actuators (SEA). (a) A typical SEA, presenting a monotonic elastic energy profile and a single equilibrium position. (b) A multistable SEA (MSEA), where the compliant element is characterised by multiple positions of equilibrium.

coupled by aluminium spokes in a double helix-like configuration. The device is capable of large deformations and can transmit forces within the range of human muscles, making it suitable for wearable robotic applications [20].

In the present paper we propose the design of an actuator made of the bistable compliant element presented in [19] in series with a geared DC motor. We refer to the bistable element as Multistable Composite Transmission (MCT) and name the resulting design a Multistable Series Elastic Actuator (MSEA).

In previous studies, we identified the dynamic properties and the impedance-rendering characteristics of our MSEA [21, 22], proposing it as an energy-efficient alternative to traditional actuators for driving an assistive device for the upper limbs.

In the following sections, we describe the working principle and properties of an MCT, building upon the work of Pirrera, Lachenal and colleagues [23, 19] which focus on modelling of MCT's static and dynamic response.

In this work, we aim at completing the picture that we introduced in the previous works. We exploit the prior knowledge to present the details of the mechanical design of the MSEA and to provide the reader with a set of tools that guide the engineering process of a multistable transmission for application in robotics. Moreover, we propose a control strategy that can efficiently cope with the nonlinearity and multistability of the MCT to control the transition between equilibrium positions, towards the exploitation of the potential of the proposed technology.

The predictable dynamics of the MCT, obtained by suitably tailoring the constituent composite materials, provides the unprecedented possibility to choose the stiffness characteristic and the position of the multiple configurations of stability, allowing to tailor the MCT's character-

istics to a specific application.

The paper is organized as follows: Section 2 introduces the concept of Multistable Composite Transmission (MCT), describes the effects of the design parameters on the elastic energy profile, and models the dynamics of the overall actuation stage. In section 3, we characterize the MCT, extrapolating a parametric model later used for a feedforward control. Section 4 presents the working principle of a novel controller for MSEAs: an outer loop uses a model-based energy profile of the MCT to control the device's convergence towards the closest stable configuration, while an inner, robust position controller ensures that the DC motor moves accurately towards the desired location. The manuscript concludes by outlining possible practical applications of MSEAs, highlighting their advantages and limitations over state of the art approaches.

2. Design

2.1. Multistable Composite Transmission (MCT) and Design Parameters

A Multistable Composite Transmission (MCT), shown in Figure 2, is made of two pre-stressed flanges of multilayered carbon fiber/epoxy laminates. The flanges are held together in a double-helix configuration by five rigid aluminium spokes to impose a highly directional deformation to the MCT. The MCT can twist around its longitudinal axis and deform to assume any intermediate state from fully coiled to fully extended, while maintaining a constant diameter: when the motor shaft rotates one end of the MCT, with the opposite extremity constrained to translating only (and not rotating), the structure twists and changes length uniquely, depending on the twist angle, ϕ, of the DC motor.

The proposed design consists of a DC motor coupled to an MCT, which converts rotational motion to linear displacement. The MCT can be designed to have different stable configurations, corresponding to distinct points of local elastic energy minima: the elastic energy function is not monotonic, but characterized by alternating valleys and peaks, or stable and unstable configurations, respectively.

Manufacturing parameters, such as the orientation of the carbon fiber layers (plies) composing the two flanges, the width and the fiber/resin tuple, are the main morphological factors that shape the MCT's elastic energy profile. The purpose of this section is to detail how such compliant elements can exhibit a wide spectrum of dynamics, if compared to the regular elastic elements employed in SEAs and VSAs. The mechanical model presented here is based upon previous work by Lachenal *et al.* [24].This model has been thoroughly validated by Lachenal and colleagues in [19], where it was shown to be in good agreement with experimentally-derived energy profiles, with a maximum amplitude error of about 10% around the point of minima but no difference in phase.

A detailed illustration of our MSEA module is shown in Figure 2: the properties of the MCT are affected by geometrical parameters such as the length of the flanges L, their width W, the height of the spokes H and, finally, by the choice of material and the orientation of the constituent layers.

The main hypothesis for modelling the MCT is that during their deformation, the flanges lie tangentially to an imaginary cylinder of constant diameter, equal to the spoke's length, $H = 2R$ (Figure 2). In other words, it is assumed that the longitudinal axis of the flanges lies exactly on helical curves of varying pitch (described by θ), on the cylindrical surface. Furthermore, because the flanges are slender, their mid-surface is assumed to bend uniformly in the longitudinal direction.

These assumptions allow to model each configuration of the MCT by only two parameters: (i) the curvature $1/R$ of the underlying cylinder and (ii) the orientation of the local axes (η, ξ) attached to each flange, defined by the angle θ.

The elastic energy of the MCT is given by the energy of each flange composing its structure [25], which is expressed as:

$$U = \frac{LW}{2} \Delta\boldsymbol{\kappa}^T \boldsymbol{D}^* \Delta\boldsymbol{\kappa}, \tag{1}$$

where L and W are the length and width of the flange respectively, $\Delta\boldsymbol{\kappa}$ is the vector of change of curvature and $\boldsymbol{D}^*$ is the reduced flexural stiffness matrix of the flange as defined by classic lamination theory [26], exhaustively described in [19]. It is worth noting that the vector $\Delta\boldsymbol{\kappa}$ depends on the pitch angle of the flanges θ (Figure 2). To find the MCT's configuration of stable equilibrium, corresponding to a minimum of its elastic energy U, one may search for points in the elastic energy landscape meeting the following conditions:

$$\frac{\partial U}{\partial \theta} = 0, \qquad \frac{\partial^2 U}{\partial \theta^2} > 0. \tag{2}$$

The pitch angle θ can be mapped to the twist angle ϕ, which is more interesting from a control perspective, using the following relation:

$$\phi = \frac{L}{R}\left(1 - \sin\theta\right), \tag{3}$$

where R is the radius of the double helix.

The following subsections present a theoretical analysis of how design factors such as the fibers arrangement and the geometry of the flanges influence the dynamic behavior of the MCT.

2.1.1. Fibers Arrangement and Elastic Energy

In composite material parlance, the arrangement of the carbon fibers layers composing each of the two flanges of the MCT is called *lay-up*, and is the factor that most affects the elastic energy profile.

A flange can be fabricated using multiple layers of carbon laminates with fibers oriented at different angles with

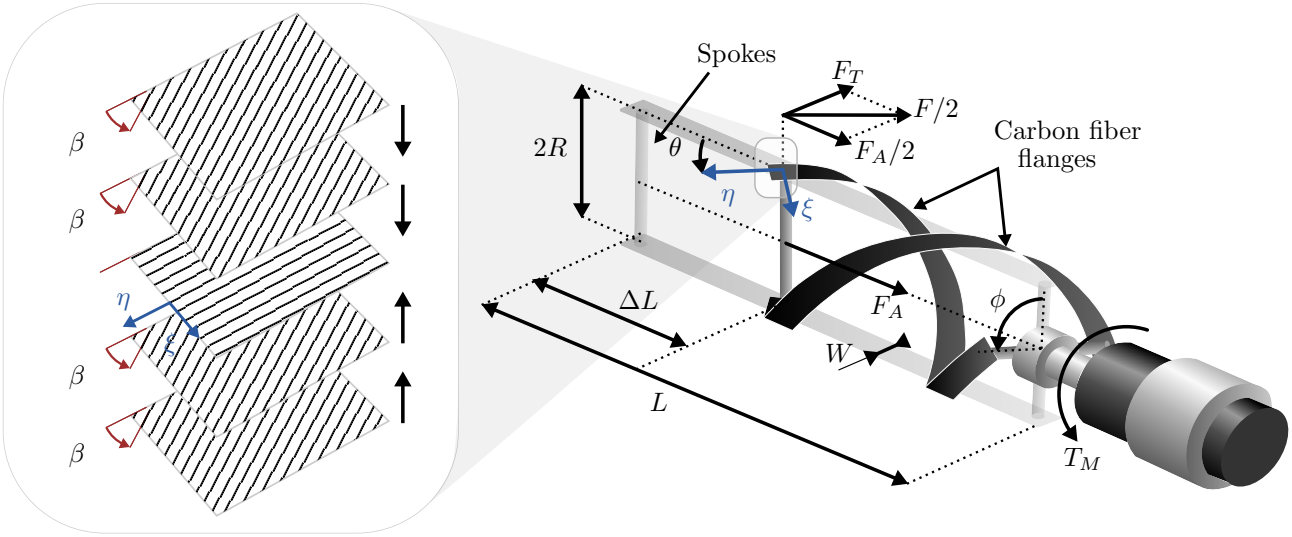

Figure 2: A multistable series elastic actuator. The multistable element is assembled by connecting two pre-stressed carbon fiber flanges with metal spokes; the structure can rotate along its main axis, converting rotary to linear motion. The zoomed area shows a detail of the lay-up, consisting of 5 carbon fiber layers arranged in symmetric manner at angles β with respect to the (η, ξ) axes.

respect to the η-axis, defining the longitudinal direction of each flange (Figure 2). Following composite laminates conventions, the lay-up is defined with numbers between square brackets, indicating the fiber orientation. In the present work, we analyse symmetric lay-ups, with the two flanges made of five layers stacked in an orientation $[\beta, \beta, 0, \beta, \beta]$, where β is a parametric angle which shapes the elastic energy and profile with respect to the twist angle ϕ of the helix.

Figure 3.a shows the influence that the lay-up parameter β plays in defining the MCT's elastic energy in an interval $\beta \in [0, \pi]$, while the twist angle varies in $\phi \in [0, 3\pi]$.

For a given β, the symmetric layup generates quasi-periodic sinusoidal strain energy functions of ϕ, meaning that the MCT assumes different configurations of stable equilibrium while it is gradually twisted along its main axis. The waveform of the elastic energy depends on the layup angle β: MCTs that have been designed with different angles β have different strain energy waveforms. In particular, from Figure 3.a, one can see that the energy assumes steeper peaks for β values closer to 0 and π, while the curve flattens for β values closer to $\pi/2$, where the difference in energy between the peaks and the valleys is less evident.

2.1.2. Dimensions of the Flanges and Elastic Energy

The MCT's characteristic dimensions L and W have a pivotal role in the design of the transmission. Let us assume that a specific symmetric layup has been chosen with β=$\pi/4$, so as to have five carbon laminates layers arranged as follows $[\pi/4, \pi/4, 0, \pi/4, \pi/4]$.

Table 1: MCT's parameters

Lay-up	β [deg]	L [mm]	W [mm]	R [mm]
symmetric	45	170	10	36

The effect of different values of L is shown in Figure 3.b, where it can be observed that longer flanges reduce the slope of the elastic energy landscape, thus leading to a more compliant transmission, in a nonlinear fashion due to Equation 3.

On the other hand, the elastic energy linearly depends on the width of the flanges W (Equation 1). Therefore, wider flanges magnify the energy excursion between peaks and valley.

We can conclude that the layup angle, β, is the only parameter affecting the topology of the stable configurations, while the magnitude of the elastic energy and therefore the level of compliance is determined by the flanges' geometry, L and W.

2.2. MSEA Assembly

In this work, we test a specific MCT design experimentally, with a set of parameters chosen before assembling the transmission. The values of the design specifications β, L, W and R are reported in Table 1.

The choice of parameters is justified by the operational workspace provided by the actuation stage to be tested. A

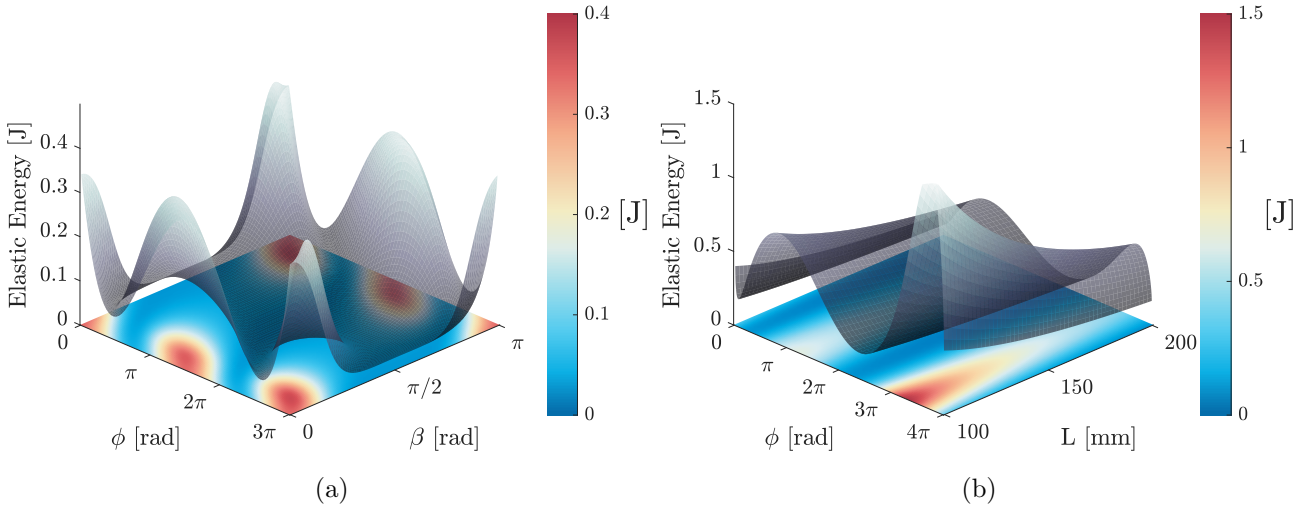

Figure 3: Elastic energy of the multistable compliant transmission for varying design parameters. (a) Elastic energy U as a function of the pitch angle ϕ and the symmetric lay-up orientation β, with $L = 170\,\text{mm}$, $W = 10\,\text{mm}$. (b) Elastic energy U as a function of ϕ and the length of the helix L for a symmetric lay-up up $[\pi/4, \pi/4, 0, \pi/4, \pi/4]$ with $W = 10\,\text{mm}$.

layup angle β of 45 deg, gives the MCT three stable equilibrium configurations. They are shown with respect to the twist angle ϕ in Figure 4.a: the equilibrium points correspond to the minima in the strain energy profile, which are found at $\phi = 0, \frac{3\pi}{2}$ and 3π. These values can be obtained by solving Equation 2. This scenario is favorable because at least one of the stable positions lies between the fully coiled and fully uncoiled configurations [19], which facilitates a bidirectional operation of the actuator. It is worth noting that the angle ϕ ranges between 0 and 3π for the set of constructive parameters listed in Table 1, as it can be observed by solving Equation 3. Theoretically, the two extreme configurations coincide but this is physically impossible due to the presence of the spokes that collide when the helix is fully coiled.

The proposed MSEA comprises a brushless DC motor, a planetary gearhead and the MCT, arranged in series. Its architecture is shown in Figure 2.a, where the MCT is connected to the motor's shaft, converting a rotary motion ϕ in a linear displacement ΔL, according to the relation:

$$\Delta L = L(1 - \cos(\theta)) \tag{4}$$

where, with reference to Figure 2, θ is the pitch angle, that can be mapped to the twist angle ϕ, using Equation 3. The chosen configuration, show in Table 1, has a stroke of $\approx$150 mm, for a twist angle between 0 rad and 3π rad.

The elastic strain U, the MCT's axial force and stiffness are shown as a function of the DC motor twist angle ϕ, in Figure 4. Upon rotation of the motor's shaft, starting from a coiled configuration, the MCT opens up to an extended stable configuration and then recoils to a third stable one. The stiffness and axial force of the MCT are shown in Figure 4.b: the stiffness of the structure increases nonlinearly from the coiled to the extended configuration, this last one being a singular position, with virtually infinite stiffness. Note that the stiffness assumes negative values, for ϕ close to 0 rad, 3π rad and soon after the singular position. In these regions, the elastic force acts in the direction of increasing angles instead of opposing motion. This nonlinearity makes the system particularly challenging to control with a simple feedback controller. Similarly, the elastic force exerted by the MCT to return to its closest stable position, increases approaching the extended shape and crosses zero in the structure's equilibrium points.

By controllng the twist angle ϕ, the role of the DC motor here is twofold: (1) it can be used to accumulate and control the rate of release of potential energy in the MCT, while changing the output position of a load between the helix's two stable states [14]; (2) it can be used to control the dynamic properties of the interaction with the environment, very much like a VSA, switching from a compliant (coiled) to a stiff (extended) interaction. Note that, in arrangement proposed in this paper, (1) and (2) cannot be achieved independently, i.e. a change in the position of a load will also lead to a change in stiffness.

In the following section we propose a characterization procedure to identify the dynamic properties of the MSEA, with the goal of designing a model-based robust controller.

3. Characterization

Figure 5.a shows the electromechanical DC motor connected to the MCT and a load. This spring-like assembly can be modelled as a one degree of freedom, second order system to simulate the dynamic response to the application of an input motor torque T_M. Mathematically this is done by solving the equation of motion of the overall actuation stage as:

$$I_\text{M}\ddot{\phi} + B_\text{M}\dot{\phi} = T_\text{M} - T_k - T_b, \tag{5}$$

where $\dot{\phi}$ and $\ddot{\phi}$ correspond to the velocity and acceleration of the twist angle of the DC motor, respectively. Of

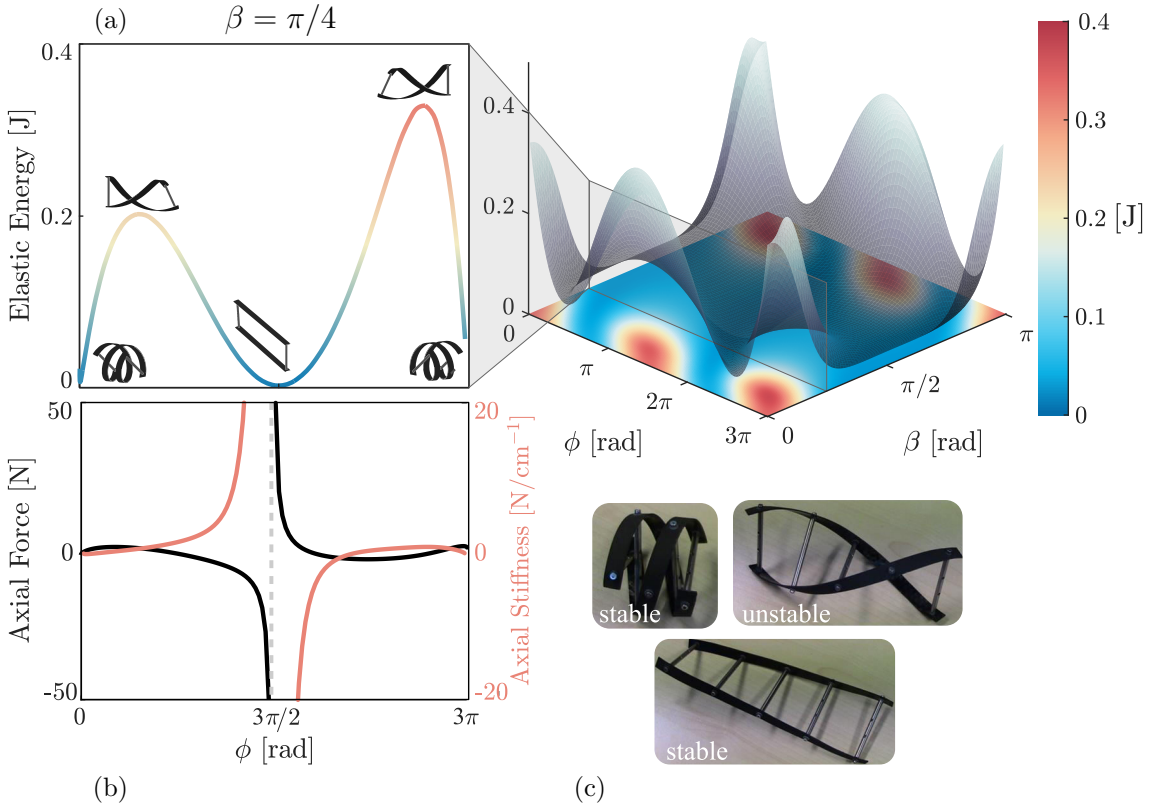

Figure 4: Equilibrium configurations, elastic and dynamic properties of the MCT as a function of the twist angle for the design parameters shown in Table 1. (a) Elastic energy profile of the MCT as function of the twist angle of the motor; note that within the span of 3π rad, the helix has five equilibrium positions, three of which stable. (b) Axial stiffness and force of the MCT: the structure's elasticity varies in a wide range, from near-zero in the fully coiled shape, to virtually rigid in the extended configuration. (c) Photos of the MCT in its equilibrium points, two of them being stable and one unstable.

the left hand side coefficients, B_{M} denotes the torsional damping of the gearbox in the motor, and I_{M} represents its moment of inertia, including the gear reduction. The torque parameters on the right hand side are defined as follows: T_{M} denotes the input torque applied by the motor; $T_k = K_\tau \phi$ and $T_b = B_\tau \dot{\phi}$ represent the elastic and damping torques generated by the MCT and K_τ and B_τ represent the torsional stiffness and damping of the MCT.

Equation (5) can be re-written in terms of an overall moment of inertia I_{A}, damping B_{A}, and stiffness K_{A} as:

$$I_{\mathrm{A}}\ddot{\phi} + B_{\mathrm{A}}\dot{\phi} + K_{\mathrm{A}}\phi = T_{\mathrm{M}} \tag{6}$$

where $I_{\mathrm{A}}{=}I_{\mathrm{M}}$, $B_{\mathrm{A}}{=}B_{\mathrm{M}} + B_\tau$, and $K_{\mathrm{A}}{=}K_\tau$.

In order to design an efficient position controller for the MSEA, the dynamic parameters I_{A}, B_{A}, and K_{A} were identified experimentally. The identification procedure consisted of applying a sinusoidal current signal to the MSEA's motor, with step-wise increasing frequency, and measuring its twist angle. During the experiment, the output of the MSEA was free to move.

The actuation stage was tested around a position of stable equilibrium ($\phi = 0$), and fitted to the model described by Equation 6. The DC motor was controlled in current mode to apply a sweep-like perturbation $T_{\mathrm{M}}(t)$, with an amplitude of 20 mN m. We tested for frequencies ranging from 1 Hz to 20 Hz, in 20 steps of 1 Hz, each held for 5 s. The output was acquired as the DC motor twist angle $\phi(t)$, read from an incremental encoder on the motor's axis.

Identification of the system's parameters was then performed via a least-squares fitting: the values of $T_{\mathrm{M}}(t)$ (input) and $\phi(t)$ (output) were collected through a Quanser data aquisition board, with a sampling frequency of 1 kHz. Equation (6) can be expressed in matrix form, correlating measurements of the system's kinematic and dynamics through N collected samples:

$$\underbrace{\begin{bmatrix} \ddot{\phi}(t_1) & \dot{\phi}(t_1) & \phi(t_1) \\ \ddot{\phi}(t_2) & \dot{\phi}(t_2) & \phi(t_2) \\ \vdots & \vdots & \vdots \\ \ddot{\phi}(t_N) & \dot{\phi}(t_N) & \phi(t_N) \end{bmatrix}}_{\boldsymbol{\Phi}} \underbrace{\begin{bmatrix} I_{\mathrm{A}} \\ B_{\mathrm{A}} \\ K_{\mathrm{A}} \end{bmatrix}}_{\boldsymbol{p}} = \underbrace{\begin{bmatrix} T_{\mathrm{M}}(t_1) \\ T_{\mathrm{M}}(t_2) \\ \vdots \\ T_{\mathrm{M}}(t_N) \end{bmatrix}}_{\mathbf{T}}. \tag{7}$$

From Equation (7), one can extract the system's parameters as:

$$\boldsymbol{p} = \left(\boldsymbol{\Phi}^T \boldsymbol{\Phi}\right)^{-1} \boldsymbol{\Phi}^T \mathbf{T} \tag{8}$$

Figure 6 shows the fitted model and collected data, in the time and frequency domains. Input (varying sinusoidal

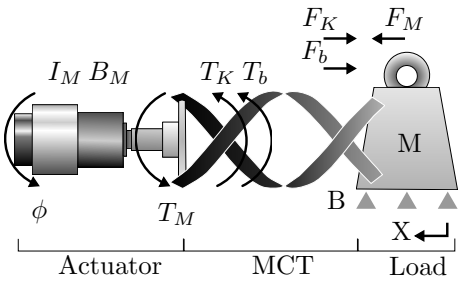

(a)

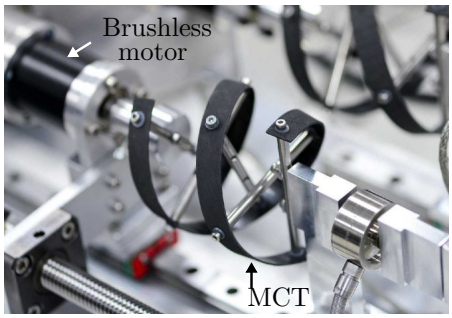

(b)

Figure 5: MSEA assembly. (a) Proposed actuation stage and dynamic terms. (b) Photo of the assembled MSEA, where the DC motor is connected to the end-effector through the MCT. When the DC motor rotates, the MCT is extends or shortens, with a linear bearing guiding the linear motion.

motor torque T_M) and measured output (angular displacement ϕ) signals were mapped to the frequency domain with a Fast Fourier Transforms (FFT).

Assuming that the system is linear around $\phi = 0$, its transfer function in the frequency domain can be expressed as:

$$H(j\omega) = \frac{\phi(j\omega)}{T_\mathrm{M}(j\omega)} \tag{9}$$

where $T_\mathrm{M}(j\omega) = \mathcal{F}\{T_\mathrm{M}(t)\}$ and $\phi(j\omega) = \mathcal{F}\{\phi(t)\}$ are the FFTs of the motor torque T_M and measured twist angle ϕ, respectively. The gain magnitude and phase of the system's transfer function are then computed as:

$$\begin{cases} G(\omega) = |H(j\omega)| \\ \varphi(\omega) = \arg(H(j\omega)) \end{cases} \tag{10}$$

The inertia, damping and stiffness were found to be, respectively, equal to $4.85 \times 10^{-5}\,\mathrm{kg\,m^2}$, $2.23 \times 10^{-3}\,\mathrm{N\,m\,s}$, and $8.66 \times 10^{-1}\,\mathrm{N\,m\,rad^{-1}}$ and were used to initialize the robust position controller described in Section 4. The Bode plots further revealed that the torque-position bandwidth of the system is about 6 Hz.

4. Control

Controlling a series elastic actuator involves an accurate knowledge of the position of the compliant element, in order to finely tune the force at the interface between the end effector and the load. When the compliant element is characterized by both elasticity and multistability, the control strategy must take into account knowledge of the elastic energy landscape across the workspace. In the arrangement proposed in this paper, one can not control the stability and the stiffness of the interaction of the MSEA independently, i.e. a change in the twist angle will cause a change in stiffness and potential energy according to the relations shown in Figure 4.

Instead of focusing on the force-control advantages of the series-elasticity, that have thoroughly been studied before [27], in this work we propose a novel strategy to make use of the MCT's multistability to control the accumulation and rate of release of elastic energy.

The control architecture uses only the encoder on the motor's axis as feedback (shown in Figure 7), with a dual purpose: (1) a stability searching algorithm is used to compute the closest configuration of equilibrium and to use the DC motor to accompany the MCT towards said configuration; this algorithm can be used to control the rate at which the MCT releases the accumulated energy or to input extra energy when the driven load is too high to be handled by the compliant element alone; (2) a robust position control, used as an inner loop of the equilibrium search algorithm, or alone to actively move the MCT from a low to a high energy state.

It is worth noting that once the actuation stage is configured in one of its minima, the MSEA is intrinsically stable and no additional effort by the DC motor is needed to hold the position.

4.1. Stability Search

The MSEA shown in Figure 5.b has three stable states, corresponding to the three local minima in the MCT's elastic energy profile (Figure 4). When positioned on a crest of potential energy, the MCT will snap to its closest equilibrium position.

We propose a control paradigm for the DC motor to accompany the MCT to its closest point of stability starting from an arbitrary twist angle ϕ. This can be useful in applications requiring low bandwidth, where one wants to control the rate at which the elastic energy is released, or when extra energy from the motor is needed to complete a task.

We do so starting from the analytical model of the elastic energy profile of the MCT, proposed and validated in [23], and use a gradient descent algorithm to compute the path towards the stable state.

Gradient descent is an iterative optimization algorithm that allows to find a point of minimum, starting from an arbitrary position, by taking steps proportional to the negative gradient of a function. In our specific case, this is done by updating, at each sampling step, the twist angle of the MCT using the following law:

$$\phi_r^{t+1} \leftarrow \phi_r^t - \lambda \nabla U \tag{11}$$

where λ is a parameter that controls the rate of convergence of the algorithm and ∇U is the derivative of the

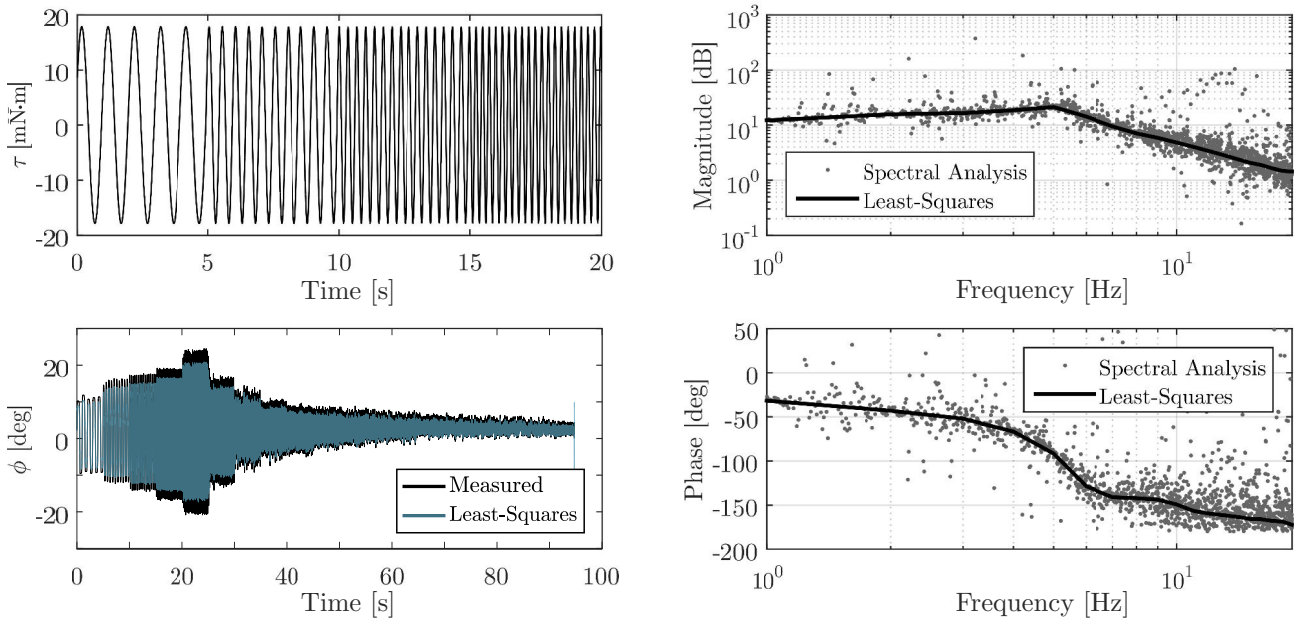

Figure 6: Characterization of the MSEA. Left portion: (top) the sine-chirp input torque with a frequency ranging from 1 Hz to 20 Hz, shown, for the sake of clarity, for the first 20 s only, and (bottom) the corresponding output twist angle $\phi(t)$, measured (black) and predicted using a least-squares identification (blue). Right portion: Bode plot of estimated system's transfer function, estimated using a least-squares method (black) and a spectral analysis (grey).

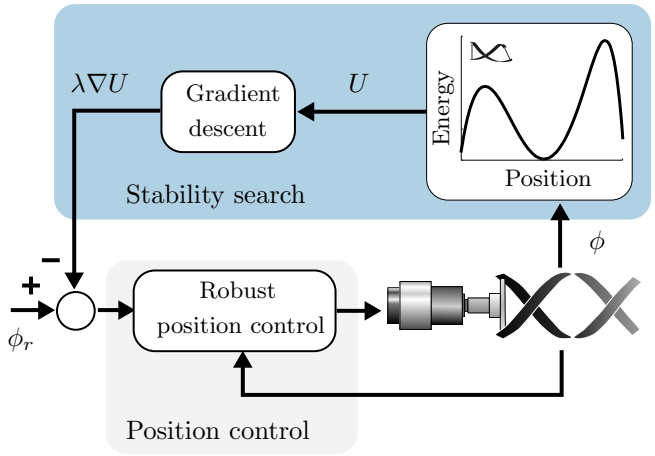

Figure 7: Control scheme for the MSEA. ϕ_r is the reference motion for the DC motor, while ϕ is the measured one, used both by the equilibrium search algorithm and by the robust position controller. The former updates the reference position to move the MCT towards a position of stable equilibrium, at a rate that can be controlled by λ. The position controller, when used alone, is adopted to move the MCT from a low to a high energy state.

elastic energy profile with respect to the twist angle ϕ, calculated by differentiating Equation 1. This new reference twist angle ϕ_r is then fed to an inner robust position control loop.

4.2. Robust Position Controller

The second block of the proposed controller is implemented to track the desired twist angle of the MCT accurately. This can be used to actively move the MCT from a low to a high energy state or to track the position reference ϕ_r, updated by the equilibrium search controller.

We propose a closed-loop robust position controller based on a Linear Kalman Filter (LKF). The Kalman filter is often used to account for variations of the system parameters and unknown external disturbances, making the controller robust to uncertainties. This approach has been successfully used in discrete acquisitions and in multi-nested closed-loop control algorithms [28].

The working principle of the overall controller is based on a state feedback technique, combined with two feed-forward compensation terms that stabilize the system and eliminate the effects of uncertainties and external disturbances. A schematics of the robust position controller is shown in Figure 8.

For the feedforward term, one needs to model the dynamics of the MSEA: the general equation of motion is derived from Equation 6, by adding an external disturbance T_{ext}, which results in:

$$T_{\text{M}} = I_{\text{A}}\ddot{\phi} + B_{\text{A}}\dot{\phi} + K_{\text{A}}\phi + T_{\text{ext}}. \tag{12}$$

In order to capture the unmodelled system's dynamics due to the nonlinear behavior of the MCT, the previously identified system parameters, i.e. inertia I_{A}, damping B_{A}, and stiffness K_{A}, are expressed in terms of means $\overline{(\cdot)}$ and

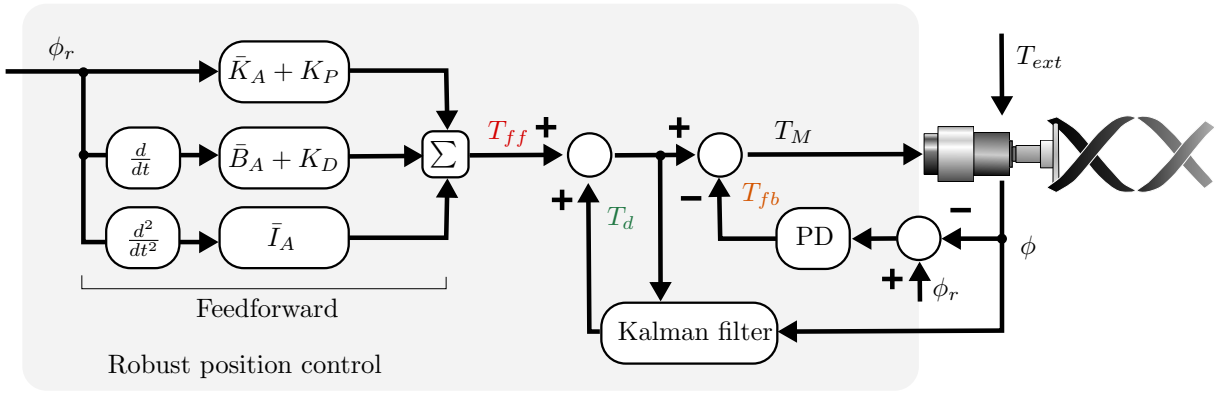

Figure 8: Robust position controller for the MCT. The proposed approach is based on three main components: a feedback term (orange), which is a linear PD control to stabilize the system, a feedforward term (red) necessary to handle the nonlinearity of the helix, and an adaptive term (green) used to compensate for the unknown system dynamics and disturbances.

variations Δ, as:

$$\begin{cases} I_{\mathrm{A}} = \overline{I}_{\mathrm{A}} + \Delta I_{\mathrm{A}} \\ B_{\mathrm{A}} = \overline{B}_{\mathrm{A}} + \Delta B_{\mathrm{A}} \\ K_{\mathrm{A}} = \overline{K}_{\mathrm{A}} + \Delta K_{\mathrm{A}} \end{cases} \tag{13}$$

where the means correspond to the values identified in the vicinity of the stable equilibrium point (cfr. Section 3) and the variations represent the unmodeled components of the system parameters that largely vary depending on the amplitude of the angle ϕ. These variations are grouped together with the external disturbances as follows:

$$D(t) = \Delta I_{\mathrm{A}}\ddot{\phi}(t) + \Delta B_{\mathrm{A}}\dot{\phi}(t) + \Delta K_{\mathrm{A}}\phi(t) + T_{\mathrm{ext}}(t), \tag{14}$$

so that, by plugging (14) in (12), T_{M} becomes:

$$T_{\mathrm{M}}(t) = \overline{I}_{\mathrm{A}}\ddot{\phi}(t) + \overline{B}_{\mathrm{A}}\dot{\phi}(t) + \overline{K}_{\mathrm{A}}\phi(t) + D(t), \tag{15}$$

This system can be modelled in the state space representation:

$$\begin{cases} \dot{\mathbf{x}}(t) = \mathbf{A}\mathbf{x}(t) + \mathbf{B}u(t) + \mathbf{E}u_{\mathrm{D}}(t) \\ \mathbf{y}(t) = \mathbf{C}\mathbf{x}(t) \end{cases} \tag{16}$$

where $\mathbf{x} = \begin{bmatrix}\phi(t) & \dot{\phi}(t)\end{bmatrix}^T$ is the state vector, $u(t) = T_{\mathrm{M}}(t)$, $u_{\mathrm{D}}(t) = D(t)$, and

$$\mathbf{A} = \begin{bmatrix} 0 & 1 \\ -\overline{K}_{\mathrm{A}}/\overline{I}_{\mathrm{A}} & -\overline{B}_{\mathrm{A}}/\overline{I}_{\mathrm{A}} \end{bmatrix}, \qquad \mathbf{B} = \begin{bmatrix} 0 \\ 1/\overline{I}_{\mathrm{A}} \end{bmatrix},$$
$$\mathbf{E} = \begin{bmatrix} 0 \\ -1/\overline{I}_{\mathrm{A}} \end{bmatrix}, \qquad \mathbf{C} = \begin{bmatrix} 1 & 0 \end{bmatrix}.$$

From the control schematic representation in Figure 8, the control signal $u(t) = T_M(t)$, sent to the DC motor, consists of three terms: one coming from the feedback loop (T_{fb} in orange) and the remaining two deriving from the feedforward control effort (T_{ff}, in red, and T_d, in green) that compensate for un-modelled dynamics and unknown external disturbances, i.e:

$$u(t) = T_{\mathrm{M}}(t) = -T_{fb}(t) + T_d(t) + T_{ff}(t), \tag{17}$$

where $T_{fb}(t)$ is a typical feedback PD controller. $T_d(t)$ is the torque used to compensate for the un-modelled dynamics, $D(t)$, and can be calculated as:

$$T_d(t) = \hat{D}(t), \tag{18}$$

where $\hat{D}(t)$ denotes the estimated value of $D(t)$. $T_{ff}(t)$ is the other feedforward compensating signal, which is computed from the reference motion $\phi_r(t)$ coming from the searching algorithm:

$$T_{ff}(t) = \overline{I}_{\mathrm{A}}\ddot{\phi}_r(t) + \left(\overline{B}_{\mathrm{A}} + K_{\mathrm{D}}\right)\dot{\phi}_r(t) + \left(\overline{K}_{\mathrm{A}} + K_{\mathrm{P}}\right)\phi_r(t), \tag{19}$$

By substituting (17)-(19) into (16), the state space equation becomes:

$$\dot{\mathbf{x}}(t) = (\mathbf{A} - \mathbf{B}\mathbf{K})\mathbf{x}(t) + \mathbf{B}\left[T_d(t) + T_{ff}(t)\right] + \mathbf{E}u_{\mathrm{D}}(t). \tag{20}$$

The unknown dynamics and external disturbance $D(t)$ can be estimated using a recursive algorithm based on the linear discrete Kalman filter: the state space model given in (20) is extended by including the total unknown component $D(t)$ as a new state variable. The model in (20) is defined in a discrete form as:

$$\begin{cases} \mathbf{x}(k+1) & = (\mathbf{A}_k - \mathbf{B}_k\mathbf{K})\,\mathbf{x}(k) + \mathbf{B}_k\left[T_d(k) + T_{ff}(k)\right] \\ \mathbf{y}(k) & = \mathbf{C}_k\mathbf{x}(k) \end{cases} \tag{21}$$

where:

$$\mathbf{x}(k) = \begin{bmatrix}\phi(k) & \dot{\phi}(k) & \hat{D}(k)\end{bmatrix}^T$$

is the new state vector including the estimated value $\hat{D}(k)$ and:

$$\mathbf{A}_k - \mathbf{B}_k\mathbf{K} = \left(1 + T_s\begin{bmatrix} 0 & 1 & 0 \\ -\frac{(\overline{K}_{\mathrm{A}}+K_{\mathrm{P}})}{\overline{I}_{\mathrm{A}}} & -\frac{(\overline{B}_{\mathrm{A}}+K_{\mathrm{D}})}{\overline{I}_{\mathrm{A}}} & -\frac{1}{\overline{I}_{\mathrm{A}}} \\ 0 & 0 & 0 \end{bmatrix}\right),$$

$$\mathbf{B}_k = T_s \begin{bmatrix} 0 \\ 1/\bar{I}_{\mathrm{A}} \\ 0 \end{bmatrix},$$

$$\mathbf{C}_k = \begin{bmatrix} 0 & 0 & 1 \end{bmatrix},$$

where $T_s = 10^{-3}$ s is the sampling rate. The output of the state space model $\mathbf{y}(k) = \hat{D}(k)$, which is estimated by LKF, is used to compensate for uncertainties and disturbance effects.

5. Experiments

5.1. Setup and Methodology

We set out to perform an experimental test to specifically compare the performance of the low-level robust control strategy as opposed to a standard PID control, tuned with the Ziegler-Nichols method, in tracking an arbitrary trajectory profile. This arbitrary trajectory profile was chosen to replicate the dynamic response of an underdamped second order system due to its inherent challenging nature. In fact, the sudden changes of direction of actuation and the consequent intense accelerations can put the controllers to the test.

The robust controller, employing a Kalman filter, is expected to outperform a simple PID, which is inherently less capable of dealing with the stiffness nonlinearities characteristic of the MCT. In order to demonstrate the ability of the system to compensate for external disturbances, a 2 Hz sine wave, 20 mN · m in amplitude was input to the actuator as an additional torque, summed to the control signal, to simulate an external torque, while the MSEA was commanded to follow an arbitrary position profile.

We conducted two additional experiments to verify the accuracy and efficacy of the proposed control architecture. These included an assessment of the position control alone, to move the MCT from a low to a high-energy state, and of the equilibrium searching algorithm, to guide the MSEA towards the closest stable position. The equilibrium searching algorithm was tested for four rates of convergence, to verify the possibility of modulating the rate of release of the elastic energy accumulated by the MCT.

The two experiments consisted in actively moving the MSEA to an unstable state, using the inner robust position loop alone, and then activating the gradient descent loop to reconfigure the MCT; each cycle was repeated 10 times. In the first experiment the system was initially moved to $\phi_r = \pi/4$, resulting in the gradient descent bringing it back to its initial position. In the second experiment, the MCT was moved to $\phi_r = 3\pi/4$, resulting in the gradient descent accompanying it to its second stable state, at $3\pi/2$.

We conducted these tests using a Maxon EC-flat 90, 60 W, with a MILE encoder (2000 counts/revolution) in a direct-drive configuration (no reduction stages between the motor and the MCT) and estimated:

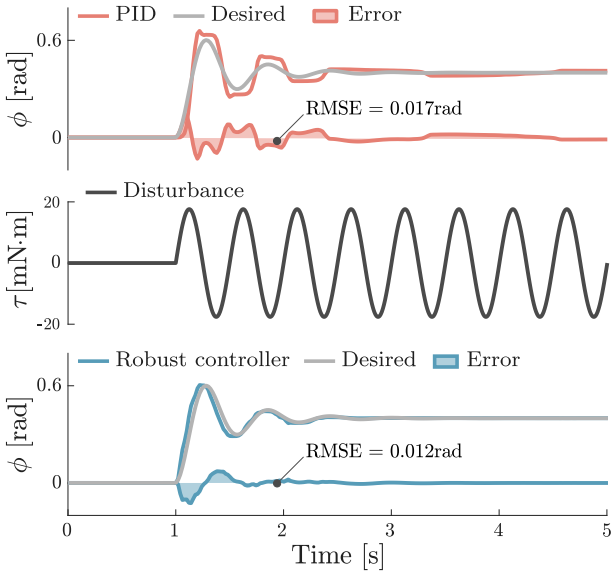

Figure 9: Performance of controller in the presence of an external disturbance. Tracking of an arbitrary motion using a conventional PID position controller (top plot) and the proposed robust position controller (bottom plot). In both conditions, a 2 Hz sine wave, starting at 1 s, was commanded to the actuator to simulate an external disturbance (middle plot).

- The torque applied by the motor: $\tau = i \times k_\tau$, where i is the motor current and k_τ its torque constant.
- The back electromotive power transmitted by the elastic element on the motor axis: $P_{emp} = i \times \omega / k_v$, where ω is the motor's velocity and k_v its speed constant.

To carry out these tests, one end of the MCT was connected to the brushless motor, while a linear bearing guided the other end along a linear trajectory (as exemplified in Figure 5). Both control and data acquisition were run on a Matlab Simulink (MathWorks, USA) environment and interfaced with a Quanser Quarc real-time workstation, at 1kHz refresh rate.

5.2. Results

Figure 9 shows that the robust controller tracks the desired trajectory with higher accuracy than a traditional PID, in both the transient and steady-state regions, resulting in a 30% improvement in tracking performance, measured by the Root Mean Square Error (RMSE) between the desired and measured profiles.

Figure 10 shows the trajectory, tracking accuracy, torque and power profiles for the first test, where the MCT was actively moved to $\phi_r = \pi/4$ (first 3 s) and then accompanied by the gradient descent towards its closest stable position, in a fully coiled state. Shaded and white areas in the plot indicate the active positioning and stability search regions, respectively.

Figure 10.a-b show the twist angle of the helix, for four different rates of convergence, and the control ac-

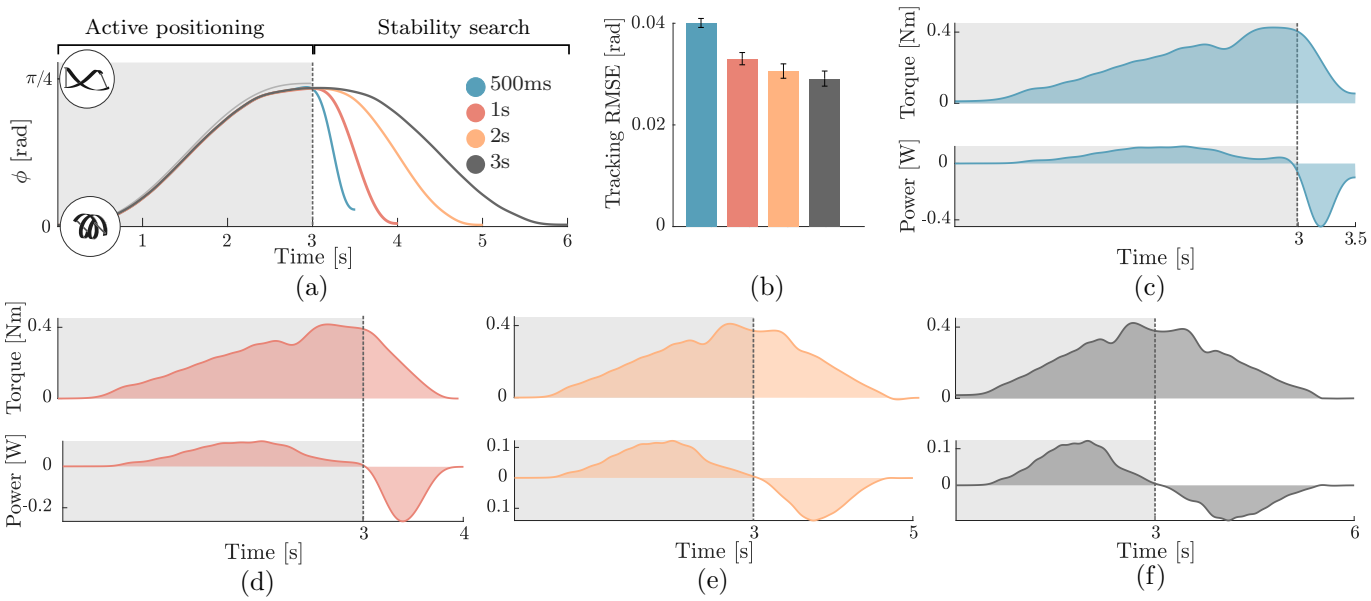

Figure 10: Reconfiguration of the MCT to the first equilibrium positions, for varying rates of convergence of the gradient descent. (a) Twist angle of the MCT for four, color coded, rates of convergence. The first 3 s, the robust position controller was used alone to reconfigure the MCT from a low to a high energy state. Once the equilibrium algorithm was turned on, the MSEA converged with a desired rate towards the closest stable position. (b) Accuracy of the low-level position controller, evaluated by the root mean squared error between the desired and measured twist angle. (c-f) Twist torque (top) and back electromotive power (bottom), for a time of convergence of 0.5,1,2 and 3 s, respectively. Note that the energy accumulated by the MCT during the loading phase is returned to aid the convergence towards equilibrium. Upon reaching the stable point, the MSEA needs no additional energy from the motor to hold the position and behaves like a SEA.

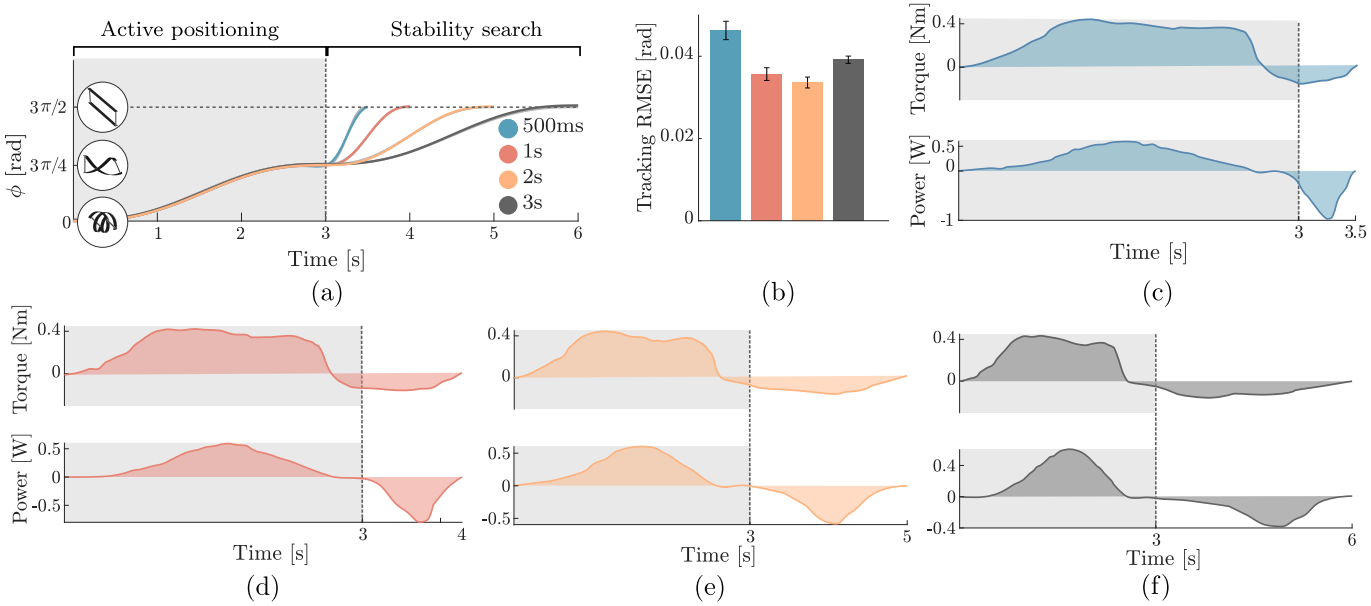

Figure 11: Reconfiguration of the MCT to the second equilibrium positions, for varying rates of convergence of the gradient descent. (a) Twist angle of the MCT. During the first 3 s, the position controller was used to actively move the MCT over the first peak of potential energy; upon turning on the gradient descent, the MSEA converged towards its second stable point. (b) Accuracy of the low-level position controller, evaluated by the root mean squared error between the desired and measured twist angle. (c-f) Twist torque (top) and back electromotive power (bottom), for a time of convergence of 0.5,1,2 and 3 s, respectively.

curacy of the low-level robust position controller, respectively. The RMSE between the desired and measured trajectories shows a velocity-dependent trend and a maximum value of (mean ± standard error of the mean) 0.040 ± 0.015 rad.The worst performance was observed for the highest convergence rate, where the gradient descent did not exactly reach the fully coiled state (light blue plot in Figure 10.a and Figure 10.c). This reflects a known behavior of gradient descent methods: high learning rates mean coarser steps towards the minimum; convergence is faster but less accurate.

The torque and power profiles are shown, for decreasing rate of convergence, in Figure 10.c-f. The torque exerted by the motor, upon turning on the stability search algorithm, gradually returns to 0, indicating that the MSEA has successfully reached an equilibrium position. The elastic energy accumulated in the positioning phase is returned to the motor in the form of back electromotive power.

A similar analysis is shown in Figure 11; this time the stability search algorithm is turned on with the MCT having a twist angle $\phi_r = 3\pi/4$, i.e. beyond the first peak of potential energy (Figure 4.a). The equilibrium search thus accompanies the elastic element, at a desired rate, towards its fully extended configuration, at $\phi_r = 3\pi/4$. The full cycle effectively results in a reconfiguration of the MSEA with very little power consumption. Tracking accuracy of the robust position controller (Figure 11.b) was lowest for high velocity, with a peak value of 0.044 ± 0.002 rad. The torque profiles (Figure 11.c-f) show a zero-crossing in the active positioning region, upon the MCT crossing a peak of potential energy. When the stability search is turned on, the torques converge to 0, indicating that the MSEA reached a configuration of equilibrium, this time in its fully extended state.

In both cases, the MSEA successfully converged to a stable configuration. The main advantage was that, after the reconfiguration, the motor could be switched off, because the system was intrinsically stable and could hold the position by relying on the structural compliance of the MCT alone.

6. Discussion

As robots increasingly cooperate with human beings, we need them to be intrinsically safe, compliant, and gentle in interacting. Adding series elasticity to traditional actuators is known to significantly improve safety, shock tolerance and force control accuracy. In this paper we presented the design of, and proposed a control strategy for, an actuator that makes use of a multistable compliant element to achieve the properties of SEAs, complementing them with higher efficiency and suitability for highly dynamic applications.

The possibility to customise the properties of an MCT makes it an extremely appealing tool. Should stability be needed when the MCT is in extended configuration, coiled or at a specific position of its stroke, one needs only to tailor the properties of its structure to suit the application. Choices such as the lay-up orientation and flanges' dimensions, governing the elastic energy profile of an MCT, can be tuned in the design phase.

These advantages come at the cost of a slight increase in control complexity. It is necessary, if such bistable structures are to be used in dynamic systems, to be able to predict their energy profile with confidence.

To increase robustness and accuracy in position- tracking, we further proposed a control strategy making use of a combined feedback and adaptive feedforward to take into account uncertainties in the model and external disturbances.

The other advantage of the MCT, that was not detailed in this work, is the high range of stiffness that can be rendered. Figure 4.b shows that, depending on the twist angle, the structure can be infinitely stiff or extremely compliant, even changing the direction of the axial force it exerts on the environment (negative stiffness). The benefits of this feature make an MSEA comparable to a VSA as a likely candidate to achieve the optimal trade-off between performance and safety proposed by Bicchi and Tonietti in [29]: the authors show that the optimal control strategy to move a mechanism between two fixed points while reducing the damage that would result from impact at any instant along its path, involves imposing a high stiffness at low velocities and a low stiffness at high velocities.

The proposed MCT provides the further benefit of converting the rotary motion of a traditional electromechanical actuator into a linear motion, eliminating the need for transmission mechanisms, e.g. spindle drives.

The major limitation of the proposed design is that one cannot modulate stiffness, position of the end-effector and equilibrium of the MCT independently. These three variables are constrained by the relations shown in Figure 4. Nevertheless, this is true only for motor-MCT arrangement shown in this paper and could be overcome by adding an extra small motor. Indeed, we are working in this direction: to design a multistable SEA where stiffness and end-effector position can be controlled independently, such as in a VSEA, but with the advantages of multistability [20].

To our knowledge this is the first application of a multistable composite material to a compliant transmission, able to generate forces and displacements suitable for assisting people in activities of daily living. We think that MSEAs could be advantageous for a variety of applications, ranging from manipulation to assistive technology. In a pick-and-place task, for example, one could make use of the binary nature of a reconfigurable bistable structure to perform an iterative task at a very low energy cost and high repeatability [14].

Similarly, the ability of the MCT to release energy at a very high bandwidth, higher than most available actuators, could be exploited to assist in human walking, running and even jumping [16]. Collins *et al.*, for instance, in their work presenting the first humanoid robot with

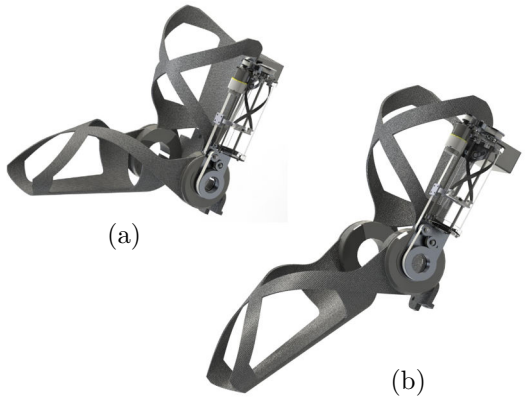

Figure 12: Concept rendering of an elbow brace employing an MSEA to assist in repetitive lifting tasks. The MCT could be here designed to be stable when the elbow is fully extended and flexed at 90 deg, as in (a). Only in the intermediate position, shown in (b), would positive power be required by the motor to surpass the MCT's crest of elastic energy.

human-like gait, highlighted the importance of a "push-off" impulse from the stance leg just before heel strike, delivered by storing elastic energy in a compliant element, using a small actuator, and releasing it in a timely manner [6]. If one designs multistable elements and shapes their elastic energy for storing torque and releasing it during propulsive phases of the walking cycle, we could decrease the amount of torque actively delivered by a motor, and design lighter, more efficient and less invasive wearable devices.

In applications requiring lower bandwidth (e.g. movements of the upper limbs), where one might need to control the rate of release of the elastic energy stored in the compliant structure, the MSEA could be used in combination with the stability search paradigm proposed herein.

A representative example could be an MSEA that helps its wearer in flexing the elbow against gravity, for aiding in repetitive lifting tasks (Figure 12). The MCT for such case could be designed to be stable both when the forearm is fully extended along the trunk and flexed at 90 deg. Positive power from the motor would only be needed in the first part of the transient lifting phase, after which the motor would only need to control the convergence of the MCT towards its second stable configuration. Upon reaching stability, the motor could be tuned off and the assistive device would passively hold the position, preserving the advantages in safety and pHRI of its compliant transmission.

7. Conclusion

The use of nonlinear, multistable elastic elements in series with a motor opens up the possibility of exploiting the existence of multiple operating conditions with inherent passive stability for improved compliance and energy efficiency; unlike traditional SEA, the device that we propose can be stable in multiple positions, that can be tailored for a specific application in the system's design phase.

The unique design we proposed paves the way for the development of new robotic actuators that sit in the border between stiff and soft robotics. In fact, we demonstrated that composite materials can be leveraged to obtain smart transmissions that achieve large forces, high tracking accuracy - that pertain to traditional robotics - upon nonlinear large structural deformations - that are typical of soft robots.

The use of nonlinear, multistable elastic elements in series with a motor opens up the possibility of exploiting the existence of multiple operating conditions with inherent passive stability for improved compliance and energy efficiency; unlike traditional SEA, the device that we propose can be stable in multiple positions, that can be tailored for a specific application in the system's design phase.

Future work will focus on the optimization of the structure, which will inherently depend on the envisioned application. Finally, we aim at adding another layer to the controller to optimize the energy storage-release cycles towards increased energy efficiency.

References

[1] A. Bicchi, M. A. Peshkin, J. E. Colgate, Safety for Physical HumanRobot Interaction, Springer Handb. Robot. (2008) 1335–1348doi:10.1007/978-3-540-30301-5_58.

[2] N. Hogan, Impedance Control: An Approach to Manipulation, in: Am. Control Conf., no. March, 1984, pp. 304–313. doi:10.1115/1.3140702.

[3] J. Salisbury, Active stiffness control of a manipulator in cartesian coordinates, in: 1980 19th IEEE Conf. Decis. Control Incl. Symp. Adapt. Process., IEEE, 1980, pp. 95–100. doi:10.1109/CDC.1980.272026.

[4] W. T. Townsend, The Effect of Transmission Design on Force-Controlled Manipulator Performance, Ph.D. thesis (1988).

[5] G. Pratt, M. Williamson, Series elastic actuators, in: Proc. 1995 IEEE/RSJ Int. Conf. Intell. Robot. Syst. Hum. Robot Interact. Coop. Robot., Vol. 1, pp. 399–406. arXiv:arXiv:1011.1669v3, doi:10.1109/IROS.1995.525827.

[6] S. H. Collins, A. Ruina, A bipedal walking robot with efficient and human-like gait, in: Proc. - IEEE Int. Conf. Robot. Autom., 2005. doi:10.1109/ROBOT.2005.1570404.

[7] E. J. Rouse, L. M. Mooney, H. Herr, Clutchable series-elastic actuator: Implications for prosthetic knee design, Int. J. Rob. Res. 33 (2014) 1611–1625. doi:10.1177/0278364914545673.

[8] N. Hogan, Adaptive Control of Mechanical Impedance by Coactivation of Antagonist Muscles, IEEE Trans. Automat. Contr.doi:10.1109/TAC.1984.1103644.

[9] G. Tonietti, R. Schiavi, A. Bicchi, Design and control of a variable stiffness actuator for safe and fast physical human/robot interaction, in: Robotics and Automation, 2005. ICRA 2005. Proceedings of the 2005 IEEE International Conference on, IEEE, 2005, pp. 526–531.

[10] S. Haddadin, A. Albu-Schäffer, G. Hirzinger, Safety evaluation of physical human-robot interaction via crash-testing., in: Robotics: Science and Systems, Vol. 3, 2007, pp. 217–224.

[11] A. De Luca, F. Flacco, A. Bicchi, R. Schiavi, Nonlinear decoupled motion-stiffness control and collision detection/reaction for the vsa-ii variable stiffness device, in: Intelligent Robots and Systems, 2009. IROS 2009. IEEE/RSJ International Conference on, IEEE, 2009, pp. 5487–5494.

[12] N. Paine, S. Oh, L. Sentis, Design and control considerations for high-performance series elastic actuators, Mechatronics, IEEE/ASME Transactions on 19 (3) (2014) 1080–1091.
[13] M. Santer, S. Pellegrino, Compliant multistable structural elements, Int. J. Solids Struct. 45 (24) (2008) 6190–6204. doi:10.1016/j.ijsolstr.2008.07.014.
[14] G. Chirikjian, A binary paradigm for robotic manipulators, Proc. 1994 IEEE Int. Conf. Robot. Autom. (July) (2014) 3063–3069. doi:10.1109/ROBOT.1994.351099.
[15] Y. Forterre, J. M. Skotheim, J. Dumals, L. Mahadevan, How the Venus flytrap snaps, Nature 433 (7024) (2005) 421–425. doi:10.1038/nature03185.
[16] M. Santer, Actuated Bistable Jumping Structures, J. Appl. Mech. 77 (3) (2010) 031009. doi:10.1115/1.4000417.
[17] M. R. Schultz, A concept for airfoil-like active bistable twisting Structures, J. Intell. Mater. Syst. Struct.doi:10.1177/1045389X06073988.
[18] M. Plooij, M. Wisse, A novel spring mechanism to reduce energy consumption of robotic arms, in: IEEE Int. Conf. Intell. Robot. Syst., 2012. doi:10.1109/IROS.2012.6385488.
[19] X. Lachenal, P. M. Weaver, S. Daynes, Multi-stable composite twisting structure for morphing applications, Proc. R. Soc. A Math. Phys. Eng. Sci. 468 (2141) (2012) 1230–1251. doi:10.1098/rspa.2011.0631.
[20] L. Cappello, A. Pirrera, P. Weaver, L. Masia, A series elastic composite actuator for soft arm exosuits: Design and preliminary test, in: Rehabilitation Robotics (ICORR), 2015 IEEE International Conference on, IEEE, 2015, pp. 61 – 66.
[21] L. Masia, L. Cappello, P. Morasso, X. Lachenal, A. Pirrera, P. Weaver, F. Mattioni, Carapace: A novel composite advanced robotic actuator powering assistive compliant exoskeleton preliminary design, in: Rehabilitation Robotics (ICORR), 2013 IEEE International Conference on, IEEE, 2013, pp. 1–8.
[22] L. Cappello, X. Lachenal, A. Pirrera, F. Mattioni, P. M. Weaver, L. Masia, Design, characterization and stability test of a multistable composite compliant actuator for exoskeletons, in: Biomedical Robotics and Biomechatronics (2014 5th IEEE RAS & EMBS International Conference on, IEEE, 2014, pp. 1051–1056.
[23] A. Pirrera, D. Avitabile, P. Weaver, On the thermally induced bistability of composite cylindrical shells for morphing structures, International Journal of Solids and Structures 49 (5) (2012) 685–700.
[24] X. Lachenal, P. M. Weaver, S. Daynes, Influence of transverse curvature on the stability of pre-stressed helical structures, International Journal of Solids and Structures 51 (13) (2014) 2479–2490.
[25] L. P. Kollár, G. S. Springer, Mechanics of composite structures, Cambridge university press, 2003.
[26] R. M. Jones, Mechanics of composite materials, Crc Press, 1998.
[27] J. Pratt, B. Krupp, C. Morse, Series elastic actuators for high fidelity force control, Ind. Rob.doi:10.1108/01439910210425522.
[28] F. Ozkul, D. Erol Barkana, Design of an admittance control with inner robust position control for a robot-assisted rehabilitation system rehabroby, in: Advanced Intelligent Mechatronics (AIM), 2011 IEEE/ASME International Conference on, IEEE, 2011, pp. 104–109.
[29] A. Bicchi, G. Tonietti, Fast and "soft-arm" tactics, IEEE Robot. Autom. Mag.doi:10.1109/MRA.2004.1310939.